

Observations of rogue seas in the Southern Ocean

A. Toffoli¹, A. Alberello², H. Clarke¹, F. Nelli³, A. Benetazzo⁴, F. Bergamasco⁵, B. Ntamba Ntamba⁶, M. Vichi^{7,8}, and M. Onorato^{9,10}

¹*Department of Infrastructure Engineering, The University of Melbourne, Parkville, VIC 3010, Australia;*

²*School of Mathematics, University of East Anglia, Norwich, United Kingdom;*

³*Department of Mechanical Engineering, Swinburne University of Technology, Melbourne, Australia*

⁴*Istituto di Scienze Marine, Consiglio Nazionale delle Ricerche, 30122 Venice, Italy*

⁵*Università Cá Foscari, 30123 Venice, Italy*

⁶*Cape Peninsula University of Technology, 7535 Cape Town, South Africa*

⁷*Department of Oceanography, University of Cape Town, Cape Town, South Africa*

⁸*Marine and Antarctic Research centre for Innovation and Sustainability, University of Cape Town, Cape Town, South Africa*

⁹*Dipartimento di Fisica, Università degli Studi di Torino, Via Pietro Giuria 1, 10125 Torino, Italy and*

¹⁰*INFN, Sezione di Torino, Via Pietro Giuria 1, 10125 Torino, Italy*

(Dated: October 4, 2023)

We report unique direct observations of surface waves from a stereo camera system aboard the South African icebreaker S.A. Agulhas II during an expedition across the Southern Ocean in the austral winter. Records include water surface elevation across a range of wave conditions, spanning from early stages of wave growth to full development. We give experimental evidence of rogue seas, i.e., sea states characterized by heavy tails of the probability density function, well beyond the expectation based on bound mode theory. These conditions emerge during wave growth, where strong wind forcing and high nonlinearity drive wave dynamics. Quasi-resonance wave-wave interactions, which are known to sustain the generation of large amplitude rogue waves, capture this behaviour. Wave statistics return to normality as the wind forcing ceases and waves switch to a full developed condition.

Ocean surface waves are driven by momentum and energy transfer through wind-induced surface pressure [1]. Under the direct action of atmospheric forcing, waves are generated and grow in height as a function of fetch, i.e., the distance over which wind blows unobstructed. Because of the four-wave resonant interactions, the peak of the wave spectrum experiences a downshift towards lower frequencies and waves become longer and faster [1]. Part of the energy is also scattered across directions, conferring a distinctive two dimensional (directional) nature to the wave energy spectrum [2]. Wave growth ceases when waves become faster than the wind, a condition which normally occurs when the wave age, i.e., the ratio of wave phase velocity (C_P) to wind speed (U), exceeds 1.25 [3].

If the wave steepness (a parameter proportional to the ratio of wave height to wavelength) is sufficiently small, the resulting ocean surface can be considered as a superposition of many wave components and its statistical framework can be approximated by a Gaussian distribution [1, 4]. In nature, however, waves are steep, and the small amplitude assumption does not always hold. Consequently, nonlinear wave-wave interactions can develop, inducing departures from Gaussian statistics [4–7]. Relative to the occurrence of extreme events, a proxy for non-Gaussian behaviours is the kurtosis [4, 7, 8], which is the forth-order moment of the probability density function of e.g. the surface elevation, and an indicator of heavy tails in the distribution.

There are two types of nonlinearities responsible for non-Gaussian statistics [9]. The first one is the result of bound modes, which make the waveform asymmetric and skew the distribution of wave amplitudes and wave

crests [10–12]. An evident, albeit weak, increment of kurtosis relative to a Gaussian random process is expected [10]. The second derives from quasi-resonant interactions between free modes, which is related to the exponential growth of a weakly modulated plane wave through the modulational or Benjamin-Feir instability [13, 14]. In a deterministic and simplified context, this instability is described by exact breather solutions of the nonlinear Schrödinger equation (NLS) [15]. These coherent oscillatory structures have been observed in several natural environments, including water, optical fibers, superfluid helium, Bose-Einstein condensates and plasmas [16–20], and they have been proposed as sensible prototypes of rogue waves, which are exceptionally large events that emerge unexpectedly amidst smaller waves [13].

Breather-like structures can develop in stochastic systems [21, 22]. If the dominant wave component is sufficiently steep, the wave spectrum is narrow-banded and propagation is unidirectional, they can occur frequently enough to cause a rogue sea state [23]. This is a conditions where wave statistics is characterised by heavy tails with strong departures from Gaussian statistics [4–6, 8, 24, 25]. The spectral density of ocean waves, however, is usually broad-banded in frequencies and spread over multiple directions [26, 27], so that the capacity to develop modulational instability is impaired [7]. Under these circumstances, theory, experiments, and numerical simulations showed that wave statistics only exhibit weakly non-Gaussian properties, deriving primarily from bound modes [4, 6, 28]. This is further supported by field observations [11, 12], even though rogue waves are present in the records [29–34].

Nevertheless, it is still unclear whether strong deviations from Gaussian statistics, well beyond the one associated to bound modes, can occur in the ocean [32]. Therefore, the framework of ocean waves in general and occurrence of extreme waves in particular remain the subject of controversy, making inclusion of extreme and rogue waves in design considerations a challenging endeavor [35, 36].

In this Letter, we discuss the statistical properties of the ocean surface elevation using field (in-situ) observations, which encompass a wide range of sea state conditions from short to long fetches. Measurements were acquired underway by a stereo camera system aboard the South African icebreaker S.A. Agulhas II during a crossing of the Southern Ocean in the austral winter (from 28 June to 13 July, 2017; Fig. 1a) [37, 38]. This remote region comprises an uninterrupted band of water around Antarctica [39]. It is dominated by strong westerly winds, the notorious roaring forties, furious fifties and screaming sixties, which give rise to some of the fiercest waves on the planet over almost infinite fetches all the year round [27, 39–41]. The average wave height in the austral winter is expected to be approximately 5 m with a 90-th percentile of about 7 m (cf., [39]).

The acquisition system consisted of two GigE monochrome industrial CMOS cameras with a 2/3 inch sensor, placed side-by-side at a distance of 4 m. The stereo rig was installed on the monkey bridge of the icebreaker approximately 25 m from the waterline and tilted 20° below the horizon. The cameras were equipped with 5 mm lenses to provide a field of view of the ocean surface $\approx 90^\circ$ around the port side of the ship. Additionally, an inertial measurement unit (IMU) was firmly attached close to the two cameras to capture the movement with respect to the sea surface during the acquisition. Images were recorded with a resolution of 2448×2048 pixels and a sampling rate of 2 Hz during daylight throughout the expedition. Images were partitioned in sequences of 30 minutes for data analysis. Complementing atmospheric data, such as true wind speed and direction, as well as navigation records, including vessel speed and heading, were acquired throughout the journey.

The open source Wave Acquisition Stereo System (WASS [42]) was used to analyse simultaneous pairs of images to find photometrically distinctive corresponding points that can be triangulated to recover their original three dimensional position in space [43], i.e., the actual surface elevation. The motion of the vessel was used to align and geo-localise data points to a common horizontal plane representing the mean sea level. The operation resolved an area of approximately $200 \text{ m} \times 200 \text{ m}$ for each stereo image (see an example of stereo pair and reconstructed surface in Fig. 1b,c), producing more than two million data points for a sequence. A detailed description of the method, including a validation against buoy data and discussion of uncertainties is reported in [40, 44]. Hereafter, we discuss a selection of sequences recorded in the open ocean with optimal light conditions

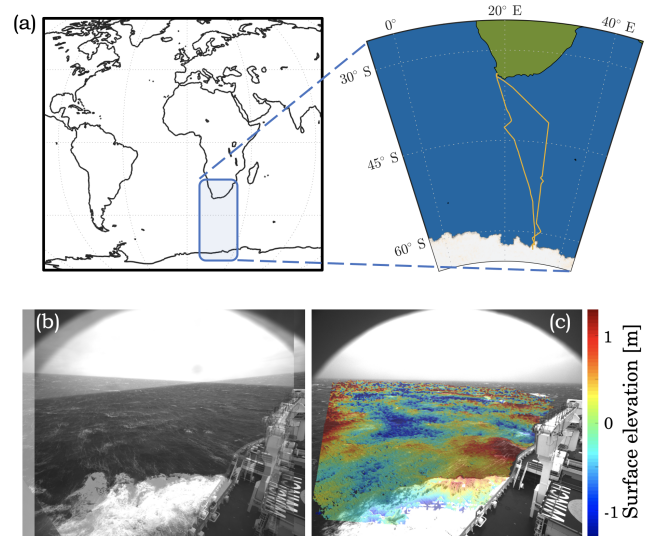


FIG. 1. Ship track (a) and sample images (b,c): example of overlapping stereo images (b) and reconstructed three dimensional surface (c)

and low uncertainties.

From each sequence, the directional wave spectrum was derived (see details in [40]) and spectral parameters were computed. These are reported in Fig. 2 as a function of the wave age relative to the spectral peak. Parameters include: the steepness, which is expressed as $\varepsilon = k_P H_s / 2$, where k_P is the wavenumber at the spectral peak, and H_s is the significant wave height computed as $4\sqrt{m_0}$, with m_0 being the zeroth order moment of the wave spectrum; the frequency bandwidth σ_f , which refers to the half width at half maximum of the dominant spectral peak relative to its peak frequency, noting that the restriction to the most energetic peak avoids ambiguities arising from the coexistence of multiple wave systems; the directional spreading σ_ϑ , which is the circular standard deviation of the directional spectrum; and the two dimensional Benjamin-Feir Index (BFI)_{2D} [7], which is calculated as

$$(BFI)_{2D} = \frac{\sqrt{2} \varepsilon}{\sigma_f} \left[\frac{1}{1 + 7R} \right], \quad (1)$$

with $R = 0.5(\sigma_\vartheta/\sigma_f)^2$. Among these parameters, the steepness is a general indicator for wave nonlinearity. Its effect on the kurtosis can be expressed as [24]

$$(\kappa)_{\text{Bound}} = 3 + 24k_P^2 m_0, \quad (2)$$

and it represents the contribution of bound waves [10]. The (BFI)_{2D}, on the other hand, is a proxy for quasi-resonant interactions between free modes [7, 13]. Their effect on the kurtosis can be calculated as [7]

$$(\kappa)_{\text{Free}} = 3 + \frac{\pi}{\sqrt{3}} (BFI)_{2D}^2, \quad (3)$$

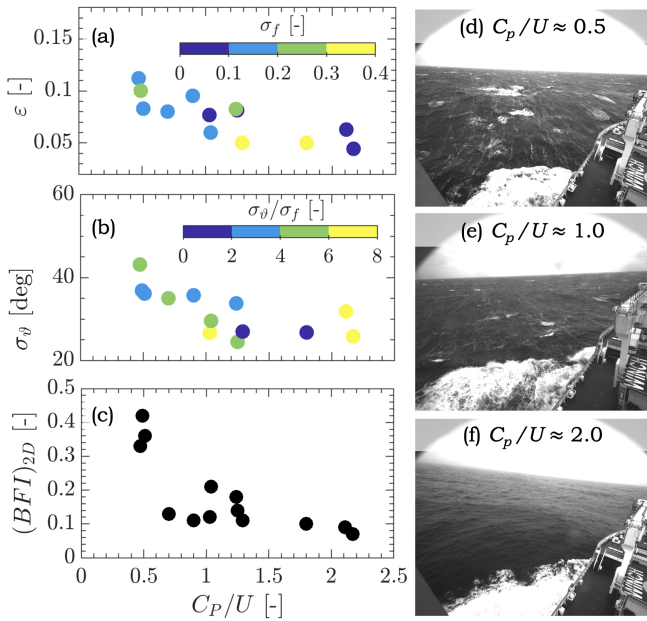


FIG. 2. Evolution of spectral characteristics across different stages of wave growth as measured by the wave age: (a) wave steepness (symbols) and frequency bandwidth (color map); (b) directional spreading (symbols) and directional spreading relative frequency bandwidth (color map); and two-dimensional Benjamin-Feir Index. Examples of sea state images at different wave age are reported: (d) growing (young) sea state ($C_P/U \approx 0.5$); (e) near fully developed sea state ($C_P/U \approx 1$); and a fully developed sea state ($C_P/U \approx 2$).

noting that significant contributions can be expected when $(BFI)_{2D} \gtrsim 1$. The overall kurtosis (κ_T) is the sum of bound and free wave contributions.

For young sea states ($C_P/U < 1$), the significant wave height varied within 3.5–4.5 m and wave period ranged 9–10 s. The waves were steep with $\varepsilon > 0.08$ (Fig. 2a), which is typical during intense storms [45] and reported during observations of extreme waves in the laboratory and in the field [2, 4, 31, 33]. However, the spectral shape was relatively broad-banded both in the frequency and directional domain (Fig. 2a,b). As the latter dominated on the former (i.e., $\sigma_\theta/\sigma_f > 1$; Fig. 2b), it follows from equation (1) that $(BFI)_{2D} \approx 0.4$ (Fig. 2c). Nevertheless, despite weak quasi-resonant interactions, the sea state retained an active nonlinearity. Consistently with laboratory experiments and numerical simulations (e.g. [46, 47]), this was demonstrated by the occurrence of whitecaps (formation of frothy, aerated crests indicating occurrence of wave breaking dissipation; see Fig. 2d) or, in some instances, multiple whitecaps recurring from the same wave train (see supplementary video [URL will be inserted by publisher]). As the sea state evolved into more mature conditions ($C_P/U \approx 1$) and eventually reached a fully developed stage ($C_P/U > 1.25$), the wave steepness gradually reduced (significant wave height ranged 2–3 m and wave period ranged 10–14 s). Concurrently, the spectral bandwidth narrowed as a combined effect of wave

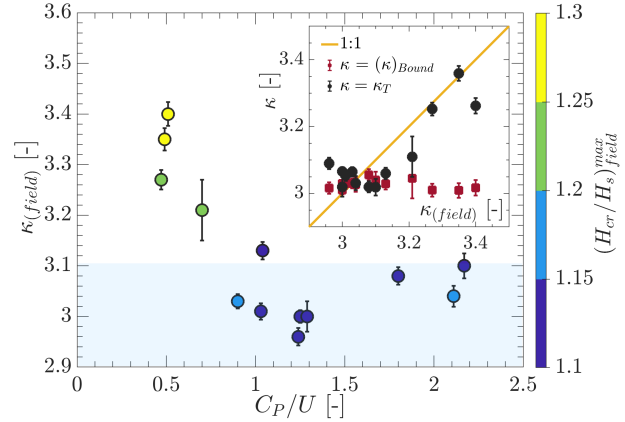


FIG. 3. Field observations of the kurtosis of the surface elevation as a function of wave age. Estimates of the maximum wave crest based on a fitted three-parameter Weibull distribution are reported as a color map. The (light blue) shaded area is shown to identify values of kurtosis normally expected for Gaussian and weakly non-Gaussian sea states. A comparison against theoretical predictions based on bound and free wave contributions is shown in the inset. The error bars represent the 95% confidence interval.

breaking, nonlinear interactions and other forms of energy dissipation such as friction at the air-sea interface and wave-induced mixing in the upper ocean [48]. It should be noted that two cases of broad spectra are reported in Fig. 2a for $C_P/U > 1$. These sea conditions are attributed to the coexistence of multiple waves system of similar peak frequency arising from rapidly veering wind. These peaks merge into a single broader spectral peak and thus go undetected by an automated analysis. Similarly to the spectral bandwidth, also the directional spreading contracted to a smaller range, in agreement with laboratory experiments [2] (see Fig. 2a,b). The $(BFI)_{2D}$ showed a distinctive decrease from ≈ 0.4 to ≈ 0.1 (Fig. 2c) due to the drop in steepness and concurrent increase of σ_θ/σ_f . Therefore, as wind forcing ceased, the nonlinear nature of the sea state faded. This was further substantiated by limited, if any, occurrence of whitecaps (see Fig. 2e,f).

Wave statistics is discussed in the form of the kurtosis of the surface elevation and it is presented in Fig. 3 as a function of wave age. Note that the kurtosis computed from observations include both bound and free wave contributions. For completeness, the maximum wave crest relative to significant wave height is also reported. In contrast to a direct estimation of the maximum crest height (i.e., maximum wave elevation) in a sequence, we extrapolated it from a surrogate statistical framework (e.g. [49]), to allow further comparison with theoretical counterparts. This was achieved by first extracting individual wave crests from time series of the surface elevation at a central location in the reconstructed image domain. A three-parameter Weibull function was then fitted to the population of observed wave crests and applied to derive

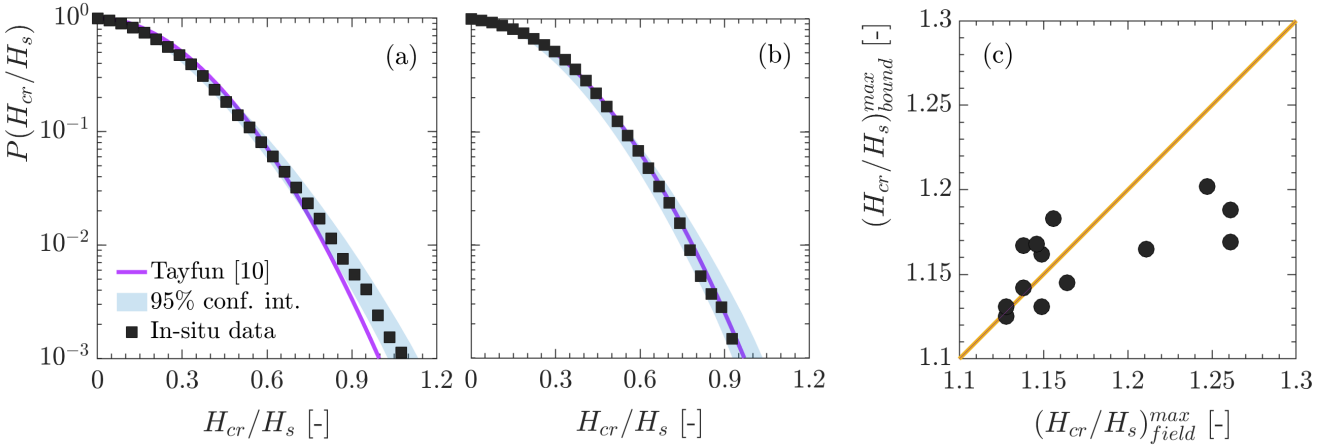


FIG. 4. Wave crest distribution in young ($C_P/U \approx 0.5$; a) and fully developed ($C_P/U \approx 2$; b) sea states from in-situ data and theory [10]. Comparison of maximum wave crest amplitudes extrapolated from in-situ data and theoretical [10] distributions (c).

a distribution of extremes as

$$F_E(H_{cr}) = \left[1 - \exp \left(- \frac{H_{cr} - \gamma_w}{\alpha_w} \right)^{\beta_w} \right]^n, \quad (4)$$

where the term within the square brackets is the three-parameter Weibull distribution, H_{cr} is a generic wave crest, and $n = 200$ denotes the number of wave crests that were, on average, included in a 30 minutes sequence. The terms α_w , β_w and γ_w are the scale, slope and location parameters of the Weibull distribution, respectively, and were estimated through a least square method. The probability of occurrence for the characteristic largest event is

$$F_E(H_{cr,max}) = 1 - \frac{1}{n}. \quad (5)$$

Therefore, by incorporating equation (4) into (5), the maximum crest can be expressed as

$$H_{cr,max} = \gamma_w + \alpha_w [\ln(n)]^{1/\beta_w}. \quad (6)$$

The kurtosis for a Gaussian or weakly non-Gaussian sea state is normally expected within 2.9–3.1 (e.g. [4]). For young sea states ($C_P/U \approx 0.5$), the kurtosis departed from this benchmark and reached values as high as 3.4. Uncertainties, as estimated in the form of 95% confidence limits through bootstrap techniques [50], were small and $\mathcal{O}(10^{-2})$. Although the probability density function of wave displacements can exhibit heavier tails and, thus, greater kurtosis in e.g. nonlinear optical fibers [13, 14, 21], the value reported herein remains significant. In the context of water waves, the most extreme events are normally restrained by breaking (see Fig. 2d), which prevents the kurtosis to increase excessively. In this regard, similar magnitudes of kurtosis were reported

in laboratory observations of highly nonlinear mechanically and wind-generated water waves [2, 4, 6]. Comparison with theoretical estimates from equations (2,3) indicates that bound wave nonlinearity cannot capture strongly non-Gaussian statistics, while quasi-resonance interactions between free waves can detect them to a certain extent (see inset in Fig. 3). As the sea state developed into more mature conditions, the kurtosis decreased exponentially, approaching Gaussian statistics already for $C_P/U \approx 1$. Theoretical estimates (2,3) are consistent with observations under these circumstances, substantiating the weak nonlinear properties of the sea state for well developed sea states.

Consistent with the high kurtosis in young seas, the estimated maximum crest height relative to the significant wave height was high and in excess of 1.2, which is the threshold identifying rogue waves (cf. [51]). Concurrently, the recovery of Gaussian statistics for mature sea states coincided with a reduction of maximum crests. Under these circumstances, crest amplitudes did not exceed the rogue wave limit.

It should be mentioned that bound waves are expected to contribute more to the wave crest statistics than kurtosis [4]. A more detailed comparison against bound wave-driven statistics, which, we recall, are the benchmark statistical framework for oceanic sea states, is reported in Fig. 4. The Tayfun distribution for wave crests [10] is assumed as reference for bound wave statistics and it is applied to equations (4,5) to extrapolate theoretical prediction of maximum crest heights [49]. For intense wind forcing ($C_P/U < 1$), the in-situ wave crest distribution shows a moderate, yet statistically significant (i.e., in excess of the the 95% confidence intervals), deviation from the theoretical counterpart (Fig. 4a). This differs from currently available field observations, which report good agreement with bound wave statistics (e.g. [11, 12, 31]).

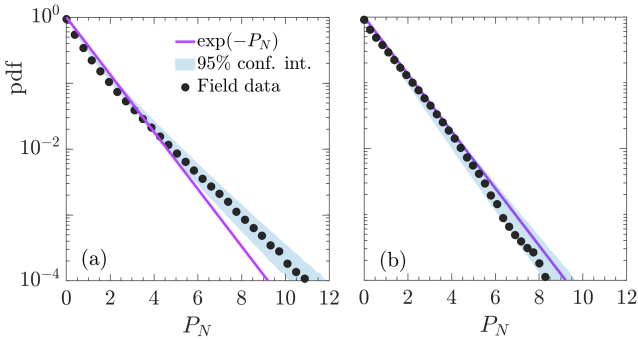


FIG. 5. Probability density function of the normalised wave intensity (P_N) for a young (a) and mature (b) seas; the 99% confidence interval is indicated as shaded (light blue) area. The young sea represents data from a sequence of image acquired for wave age $C_P/U \approx 0.5$; the mature sea represents data from a sequence of image acquired for wave age $C_P/U > 1$. The $\exp(-P_N)$, which represents a Gaussian process, is reported for benchmark.

It follows that bound waves tend to under estimate the amplitude of the most extreme crests during the growing phase of wind-generated fields (see data point referring to relative crest height in the field greater than 1.2 in Fig. 4c). As the sea state evolves into a fully developed form, departures from theoretical predictions fade: the empirical wave crest statistics match the Tayfun distribution (Fig. 4b); and extreme crest amplitudes reported in the field become consistent with theoretical predictions (see data point for relative wave crest height in the field lower than 1.2 in Fig. 4c).

For completeness, Fig. 5 shows the probability density functions of the normalised wave intensity P_N , which is the square modulus of the wave envelope normalised by its average. This is preferred to the wave displacements (surface elevation), as it better represents the upper tail of the distribution [52]. Furthermore, the wave envelope encompasses the whole reconstructed ocean surface, unlike the point approach used to extrapolate bound wave driven statistical properties. For young seas (Fig. 5a), a significant departure from the distribution of P_N expected for Gaussian statistics, i.e., $\exp(-P_N)$ [2], is evident, confirming the robustness of the heavy tail. For mature sea conditions (Fig. 5b), the distribution aligns to $\exp(-P_N)$ more closely, substantiating the Gaussian nature of fully developed wave fields. Nevertheless, it is worth mentioning that the $\exp(-P_N)$ tends to slightly over estimate the distribution of in-situ data, a feature which is attributed to the broad-banded nature of the wave fields (e.g. [29]).

In summary, we presented an unprecedented set of direct (in-situ) observations of ocean surface displacements to discuss the occurrence of large amplitude (rogue)

waves and concurrent emergence of non-Gaussian properties in wind-forced wave fields. Records comprised of a wide range of sea states from the Southern Ocean, spanning from early stages of wave development (young seas), where wave dynamics are driven by wind forcing, to fully developed stages (mature seas), where wave dynamics are no longer under the direct effect of wind. Observations revealed that large waves occurred frequently enough to prompt evident non-Gaussian statistics in young sea states. Under these circumstances, the ocean surface exhibited a clear nonlinear nature through the occurrence of wave breaking, which is a manifestation of modulational instability in a deep water regime as substantiated in laboratory and numerical tests [46, 47]. Concurrently, quasi-resonant interactions between free waves could capture, to a certain extent, this non-Gaussian behaviour. Statistically significant departures from weakly non-Gaussian statistics, which are assumed as benchmark for ocean waves, were also reported, further demonstrating a robust non-Gaussian nature of the wave field and confirming earlier results in a wind-wave flumes [2]. Conversely, as waves reached full development, effect of wind forcing faded and so did the occurrence of large waves, with statistics resuming the expected weakly non-Gaussian behaviour. The myth of rogue waves, the challenge of explaining their origin and the necessity to understand their statistics have fascinated many different fields of physics and engineering for decades. The observations presented herein are, to the best of our knowledge, the first robust evidence that ocean waves can develop into a strongly non-Gaussian process, as theory would indeed predict, when actively forced by wind. Our results casts new light onto oceanic rogue waves and has the potential to advance our current understanding and capacity to predict this mariner's myth.

ACKNOWLEDGMENTS

The expeditions were funded by the South African National Antarctic Programme through the National Research Foundation. AA and AT were funded by the ACE Foundation and Ferring Pharmaceuticals and the Australian Antarctic Science Program (project 4434). AT is supported by the Australia Research Council (DP200102828, LP210200927). AA acknowledges support from the London Mathematical Society (Scheme 5 – 52206). MV was supported by the NRF SANAP contract UID118745. We are indebted to Captain Knowledge Bengu and the crew of the SA Agulhas II for their invaluable contribution to data collection. M.O. was funded by Progetti di Ricerca di Interesse Nazionale (PRIN) (Project No. 2020X4T57A and 2022WKRYNL) and by the Simons Foundation, Award 652354 on Wave Turbulence. We acknowledge Dr L. Fascatte for technical support.

[1] P. Janssen and P. A. Janssen, *The interaction of ocean waves and wind* (Cambridge University Press, 2004).

[2] A. Toffoli, D. Proment, H. Salman, J. Monbaliu, F. Frascoli, M. Dafilis, E. Stramignoni, R. Forza, M. Manfrin, and M. Onorato, Wind generated rogue waves in an annular wave flume, *Physical review letters* **118**, 144503 (2017).

[3] G. J. Komen, L. Cavaleri, M. Donelan, K. Hasselmann, S. Hasselmann, and P. Janssen, Dynamics and modelling of ocean waves, *Dynamics and Modelling of Ocean Waves*, by GJ Komen and L. Cavaleri and M. Donelan and K. Hasselmann and S. Hasselmann and PAEM Janssen, pp. 554. ISBN 0521577810. Cambridge, UK: Cambridge University Press, August 1996. , 554 (1996).

[4] M. Onorato, L. Cavaleri, S. Fouques, O. Gramstad, P. A. E. M. Janssen, J. Monbaliu, A. R. Osborne, C. Pakozdi, M. Serio, C. Stansberg, A. Toffoli, and K. Trulsen, Statistical properties of mechanically generated surface gravity waves: a laboratory experiment in a 3D wave basin, *J. Fluid Mech.* **627**, 235 (2009).

[5] P. A. E. M. Janssen, Nonlinear four-wave interactions and freak waves, *J. Phys. Oceanogr.* **33**, 863 (2003).

[6] T. Waseda, T. Kinoshita, and H. Tamura, Evolution of a random directional wave and freak wave occurrence, *Journal of Physical Oceanography* **39**, 621 (2009).

[7] N. Mori, M. Onorato, and P. A. E. M. Janssen, On the estimation of the kurtosis in directional sea states for freak wave forecasting, *Journal of Physical Oceanography* **41**, 1484 (2011).

[8] F. Fedele, On the kurtosis of deep-water gravity waves, *Journal of Fluid Mechanics* **782**, 25 (2015).

[9] P. A. Janssen, On some consequences of the canonical transformation in the hamiltonian theory of water waves, *Journal of Fluid Mechanics* **637**, 1 (2009).

[10] M. A. Tayfun, Narrow-band nonlinear sea waves, *J. Geophys. Res.* **85**, 1548 (1980).

[11] G. Z. Forristall, Wave crest distributions: Observations and second-order theory, *J. Phys. Oceanogr.* **30**, 1931 (2000).

[12] A. Toffoli, J. Monbaliu, M. Onorato, A. R. Osborne, A. V. Babanin, and E. M. Bitner-Gregersen, Second-order theory and setup in surface gravity waves: a comparison with experimental data, *Journal of Physical Oceanography* **37**, 2726 (2007).

[13] M. Onorato, S. Residori, U. Bortolozzo, A. Montina, and F. Arechi, Rogue waves and their generating mechanisms in different physical contexts, *Physics Reports* **528**, 47 (2013).

[14] J. M. Dudley, G. Genty, A. Mussot, A. Chabchoub, and F. Dias, Rogue waves and analogies in optics and oceanography, *Nature Reviews Physics* **1**, 675 (2019).

[15] N. N. Akhmediev, V. M. Eleonskii, and N. E. Kulagin, Exact first-order solutions of the nonlinear schrödinger equation, *Theoretical and mathematical physics* **72**, 809 (1987).

[16] A. Chabchoub, N. P. Hoffmann, and N. Akhmediev, Rogue wave observation in a water wave tank, *Phys. Rev. Lett.* **106**, 204502 (2011).

[17] D. R. Solli, C. Ropers, P. Koonath, and B. Jalali, Optical rogue waves, *Nature* **450**, 1054 (2007).

[18] A. N. Ganshin, V. B. Efimov, G. V. Kolmakov, L. P. Mezhov-Deglin, and P. V. E. McClintock, Observation of an inverse energy cascade in developed acoustic turbulence in superfluid helium, *Physical Review Letters* **101**, 065303 (2008).

[19] Y. V. Bludov, V. Konotop, and N. Akhmediev, Matter rogue waves, *Physical Review A* **80**, 033610 (2009).

[20] Y.-Y. Tsai, J.-Y. Tsai, and L. I, Generation of acoustic rogue waves in dusty plasmas through three-dimensional particle focusing by distorted waveforms, *Nature Physics* **12**, 573 (2016).

[21] R. El Koussaifi, A. Tikan, A. Toffoli, S. Randoux, P. Suret, and M. Onorato, Spontaneous emergence of rogue waves in partially coherent waves: A quantitative experimental comparison between hydrodynamics and optics, *Physical Review E* **97**, 012208 (2018).

[22] J. Wang, Q. W. Ma, S. Yan, and A. Chabchoub, Breather rogue waves in random seas, *Physical Review Applied* **9**, 014016 (2018).

[23] M. Onorato, A. R. Osborne, M. Serio, and L. Cavaleri, Modulational instability and non-gaussian statistics in experimental random water-wave trains, *Physics of Fluids* **17** (2005).

[24] N. Mori and P. A. E. M. Janssen, On kurtosis and occurrence probability of freak waves, *Journal of Physical Oceanography* **36**, 1471 (2006).

[25] P. Walczak, S. Randoux, and P. Suret, Optical rogue waves in integrable turbulence, *Physical Review Letters* **114**, 143903 (2015).

[26] I. Teutsch and R. Weisse, Rogue waves in the southern north sea—the role of modulational instability, *Journal of Physical Oceanography* **53**, 269 (2023).

[27] M. H. Derkani, A. Alberello, F. Nelli, L. G. Bennetts, K. G. Hessner, K. MacHutchon, K. Reichert, L. Aouf, S. S. Khan, and A. Toffoli, Wind, waves, and surface currents in the southern ocean: Observations from the antarctic circumnavigation expedition, *Earth System Science Data* , 1 (2021).

[28] H. Socquet-Juglard, Probability distributions of surface gravity waves during spectral changes, .

[29] N. Mori, P. C. Liu, and T. Yasuda, Analysis of freak wave measurements in the sea of japan, *Ocean Engineering* **29**, 1399 (2002).

[30] M. A. Donelan and A.-K. Magnusson, The making of the andrea wave and other rogues, *Scientific reports* **7**, 1 (2017).

[31] J. Gemmrich and L. Cicon, Generation mechanism and prediction of an observed extreme rogue wave, *Scientific Reports* **12**, 1 (2022).

[32] F. Fedele, J. Brennan, S. Ponce de León, J. Dudley, and F. Dias, Real world ocean rogue waves explained without the modulational instability, *Scientific reports* **6**, 27715 (2016).

[33] E. Bitner-Gregersen, L. Fernández, J. Lefèvre, J. Monbaliu, and A. Toffoli, The north sea andrea storm and numerical simulations, *Natural Hazards and Earth System Sciences* **14**, 1407 (2014).

[34] A. Benetazzo, F. Barbariol, F. Bergamasco, A. Torsello, S. Carniel, and M. Sclavo, Observation of extreme sea waves in a space-time ensemble, *J. Phys. Oceanogr.* **45**, 2261 (2015).

[35] E. M. Bitner-Gregersen and A. Toffoli, Occurrence of rogue sea states and consequences for marine structures, *Ocean Dynamics* **64**, 1457 (2014).

[36] E. M. Bitner-Gregersen, S. K. Bhattacharya, I. K. Chatjigeorgiou, I. Eames, K. Ellermann, K. Ewans, G. Hermanski, M. C. Johnson, N. Ma, C. Maisondieu, A. Nilva, I. Rychlik, and T. Waseda, Recent developments of ocean environmental description with focus on uncertainties, *Ocean Engineering* **86**, 26 (2014), uncertainty Modelling for Ships and Offshore Structures.

[37] A. Alberello, M. Onorato, F. Frascoli, and A. Toffoli, Observation of turbulence and intermittency in wave-induced oscillatory flows, *Wave Motion* **84**, 81 (2019).

[38] M. Vichi, C. Eayrs, A. Alberello, A. Bekker, L. Bennetts, D. Holland, E. de Jong, W. Joubert, K. MacHutchon, G. Messori, *et al.*, Effects of an explosive polar cyclone crossing the antarctic marginal ice zone, *Geophysical Research Letters* **46**, 5948 (2019).

[39] I. R. Young, E. Fontaine, Q. Liu, and A. V. Babanin, The wave climate of the southern ocean, *Journal of Physical Oceanography* **50**, 1417 (2020).

[40] A. Alberello, L. G. Bennetts, M. Onorato, M. Vichi, K. MacHutchon, C. Eayrs, B. N. Ntamba, A. Benetazzo, F. Bergamasco, F. Nelli, *et al.*, Three-dimensional imaging of waves and floes in the marginal ice zone during a cyclone, *Nature communications* **13**, 1 (2022).

[41] F. Barbariol, A. Benetazzo, L. Bertotti, L. Cavalieri, T. Durrant, P. McComb, and M. Sclavo, Large waves and drifting buoys in the southern ocean, *Ocean Engineering* **172**, 817 (2019).

[42] F. Bergamasco, A. Torsello, M. Sclavo, F. Barbariol, and A. Benetazzo, WASS: An open-source pipeline for 3D stereo reconstruction of ocean waves, *Computers & Geosciences* **107**, 28 (2017).

[43] A. Benetazzo, Measurements of short water waves using stereo matched image sequences, *Coastal engineering* **53**, 1013 (2006).

[44] A. Benetazzo, B. Francesco, F. Bergamasco, A. Torsello, S. Carniel, and M. Sclavo, Stereo wave imaging from moving vessels: Practical use and applications, *Coastal Engineering* **109**, 114 (2016).

[45] A. Toffoli, J. Lefevre, E. Bitner-Gregersen, and J. Monbaliu, Towards the identification of warning criteria: analysis of a ship accident database, *Applied Ocean Research* **27**, 281 (2005).

[46] T. Waseda and M. P. Tulin, Experimental study of the stability of deep-water wave trains including wind effects, *Journal of Fluid Mechanics* **401**, 55 (1999).

[47] A. Iafrati, A. Babanin, and M. Onorato, Modulational instability, wave breaking, and formation of large-scale dipoles in the atmosphere, *Physical review letters* **110**, 184504 (2013).

[48] J. E. Stopa, F. Arduin, R. Husson, H. Jiang, B. Chapron, and F. Collard, Swell dissipation from 10 years of envisat advanced synthetic aperture radar in wave mode, *Geophysical Research Letters* **43**, 3423 (2016).

[49] A. Toffoli, M. Onorato, E. Bitner-Gregersen, A. R. Osborne, and A. Babanin, Surface gravity waves from direct numerical simulations of the euler equations: a comparison with second-order theory, *Ocean Engineering* **35**, 367 (2008).

[50] G. James, D. Witten, T. Hastie, and R. Tibshirani, *An introduction to statistical learning*, Vol. 112 (Springer, 2013).

[51] M. Christou and K. Ewans, Field measurements of rogue water waves, *Journal of physical oceanography* **44**, 2317 (2014).

[52] P. A. E. M. Janssen, On a random time series analysis valid for arbitrary spectral shape, *Journal of Fluid Mechanics* **759**, 236 (2014).